Effects of Longitudinal Beam Compression in a Free-Electron Laser

C. W. Roberson[1] and B. Hafizi[2,*]

[1]*Physics Division, Office of Naval Research, Arlington, Virginia 22217*

[2]*Beam Physics Branch, Naval Research Laboratory, Washington, D.C. 20375*

(Received 6 August 1993)

When the scaled growth rate of a free-electron laser (FEL) is plotted as a function of the scaled thermal velocity for the case of ideal beam compression, we find two distinct cases. If the FEL is in the energy-spread-dominated regime, the growth rate can be improved as a result of compression provided the scaled thermal velocity is less than unity. Surprisingly, we find that the growth rate is always improved if the FEL is in the emittance-dominated regime.

PACS numbers: 41.60.Cr

Since the gain of a free-electron laser (FEL) increases with current [1], a number of schemes have been proposed to increase the current from the accelerator by compressing the beam in the axial direction [2–7]. However, phase space density conservation implies that the velocity spread in the axial direction must increase, which tends to reduce the growth rate due to kinetic effects [8]. So the following questions arise. Does beam compression help? If so, when and by how much? To answer these questions we characterize the axial component of beam quality by the scaled thermal velocity,

$$S \equiv \frac{\beta_{\mathrm{th},z}}{\langle \beta_z - \beta_{\mathrm{ph}} \rangle} . \tag{1}$$

Here, β_z is the axial velocity of an electron, β_{ph} is the phase velocity of the *fastest* growing ponderomotive wave, $\beta_{\mathrm{th},z} \equiv \langle (\beta_z - \langle \beta_z \rangle)^2 \rangle^{1/2}$ is the root-mean-square (rms) spread in the axial velocity, $\langle \cdots \rangle$ indicates the mean over the electron distribution, and all the velocities are normalized to the speed of light *in vacuo*, c. If the FEL is in the energy-spread-dominated regime, compression is useful provided $S \leq 1$ initially; for larger S, compression actually reduces the growth rate. Surprisingly, if the beam is in the emittance-dominated regime, compression always enhances the growth rate. It is shown here that one can determine *a priori* the usefulness of beam compression for a given experiment. Further, it is shown that the scaled thermal velocity provides a useful measure of the axial component of the FEL beam quality and a physical interpretation of the results. For the examples considered, a peak improvement in the growth rate by a factor ~ 2 is obtained when the current is increased by a factor ~ 10–20. The effect of compression on the growth rate S, filling factor, and radius of curvature of the radiation wave fronts has been calculated and displayed graphically for several examples.

The analysis of longitudinal beam compression proceeds by making two assumptions. First, in an ideal compression scheme the charge in a micropulse is conserved. If l is the bunch length and I is the current, this constraint is expressed as

$$lI = \mathrm{const} . \tag{2}$$

Second, adapting Liouville's theorem to the six-dimensional phase space of noninteracting electrons, the invariance of normalized emittance implies conservation of longitudinal phase space:

$$l p_{\mathrm{th},z} = \mathrm{const} , \tag{3}$$

where $p_{\mathrm{th},z}$ is the rms spread in p_z. Note that Eq. (3) embodies what is meant by an ideal compression scheme, that is, neglecting all other effects that are expected to *increase* phase space volume. When the electron beam is compressed by a factor α, Eqs. (2) and (3) imply the following transformations in the FEL parameters:

$$I = \alpha (I)_0 ,$$

$$\frac{\sigma_\gamma}{\gamma_0 D} = \sqrt{\alpha} \left(\frac{\sigma_\gamma}{\gamma_0 D} \right)_0 ,$$

$$\frac{k_{\beta 0}}{k_w D} = \frac{1}{\sqrt{\alpha}} \left(\frac{k_{\beta 0}}{k_w D} \right)_0 ,$$

where $(\,)_0$ on the right hand side indicates the value prior to compression.

To define the notation used, an outline of the FEL model follows [9,10]. A matched electron beam-optical beam system is assumed to propagate along the z axis of a planar wiggler. The wiggler vector potential is given by $\mathbf{A}_w = A_w \cosh(k_w y) \sin(k_w z) \mathbf{e}_x$, where A_w is the amplitude, $2\pi/k_w$ is the period, and $\mathbf{e}_x$ is the unit vector along the x axis. The vector potential of the optically guided radiation beam is given by $\mathbf{A}_s = \frac{1}{2} A_s(y) \exp[i(kz - \omega t)] \mathbf{e}_x + \mathrm{c.c.}$, where ω is the angular frequency, $A_s(y)$ is the amplitude, and k is the complex-valued wave number which is to be determined. Short-pulse effects, such as spiking, are neglected.

The FEL Hamiltonian function $-p_z(y,p_y;t,-E;z)$ is given by

$$p_z \approx E/c - (m^2 c^3/2E) \left\{ 1 + \frac{p_y^2 + P_x^2}{m^2 c^2} + \frac{a_w^2}{2} [1 + (k_w y)^2] + \frac{a_w a_s}{2i} f_B \exp[i(k + k_w) z - i\omega t] + \mathrm{c.c.} \right\} ,$$

where $E \equiv \gamma mc^2$ is the energy, m is the mass, $-|e|$ is the charge on an electron, t is the time, (P_x, p_y) are the momenta

0031-9007/94/72(11)/1654(4)$06.00

conjugate to the coordinates (x,y), $a_{w,s}=|e|A_{w,s}/mc^2$, $f_B=J_0(\xi)-J_1(\xi)$ is the usual difference of Bessel functions, and $\xi=(a_w/2)^2/(1+a_w^2/2)$. In the betatron phase space, $J\equiv\int\int dy\,dp_y/2\pi$ is the action invariant and $k_\beta=a_w k_w/\sqrt{2}\gamma$ is the betatron wave number.

The equilibrium electron distribution is a function of the constants of motion:

$$F(E,P_x,J)=n_{b0}\frac{\exp[-(\gamma-\gamma_0)^2/\sigma_\gamma^2]}{\sqrt{\pi}\sigma_\gamma mc^2}\times\delta(P_x)\frac{\exp(-\sqrt{2}J/a_w k_w mc\sigma_b^2)}{\sqrt{\pi}a_w k_w mc\sigma_b},$$

where $\gamma_0 mc^2$ is the mean energy, $\sigma_\gamma mc^2$ is the energy spread, and $n_b(y)=n_{b0}\exp(-y^2/2\sigma_b^2)$ is the spatial density, with peak value n_{b0} and width σ_b.

The eigenvalue k is obtained by a variational principle with trial function $a_s(y)=\exp(-k_s y^2/2\zeta_R)$. Here, $k_s=2\gamma_0^2 k_w/(1+a_w^2/2)$ is the wave number corresponding to the mean electron energy, $\zeta_R\equiv k_s(2/\sigma_s^2+ik_s/R)^{-1}$ is the variational parameter, σ_s is the spot size of the optical beam, and R is the radius of curvature of the wave fronts. Rather than k, it is more convenient to consider the dispersion relation for μ, defined by $k=\omega/c-\mu k_w$, as indicated in Refs. [9] and [10]. The key variables in the dispersion relation are the unnormalized emittance, $\epsilon=k_{\beta0}\sigma_b^2$ and the "transverse current,"

$$D=\left[\left(\frac{2\pi}{k_{\beta0}k_s}\right)^{1/2}\frac{I}{I_A}\frac{a_w^2}{1+a_w^2/2}\right]^{1/2}f_B, \tag{4}$$

where $I_A=1.7\times10^4\gamma_0\beta_{z0}$ A is the Alfvén current, I is the current per unit length, and $k_{\beta0}$ is the betatron wave number evaluated at γ_0.

The dispersion relation and the equation obtained by equating its derivative to zero determine μ and ζ_R in terms of several *universal* scaled parameters. The scaled wiggler amplitude is $k_{\beta0}/k_w D$; the real and imaginary parts of μ/D represent the wave-number shift and growth rate, respectively; the pair σ_b/σ_s and $k_{\beta0}R$ denote the filling factor and scaled radius of curvature, respectively; finally, the scaled emittance is $k_s\epsilon$ and the scaled energy spread is $\sigma_\gamma/\gamma_0 D$. Presenting the results in terms of universal parameters has the merit of being applicable to all FELs. Typically in experiments D is small compared to unity. This is also the regime of validity of the present analysis.

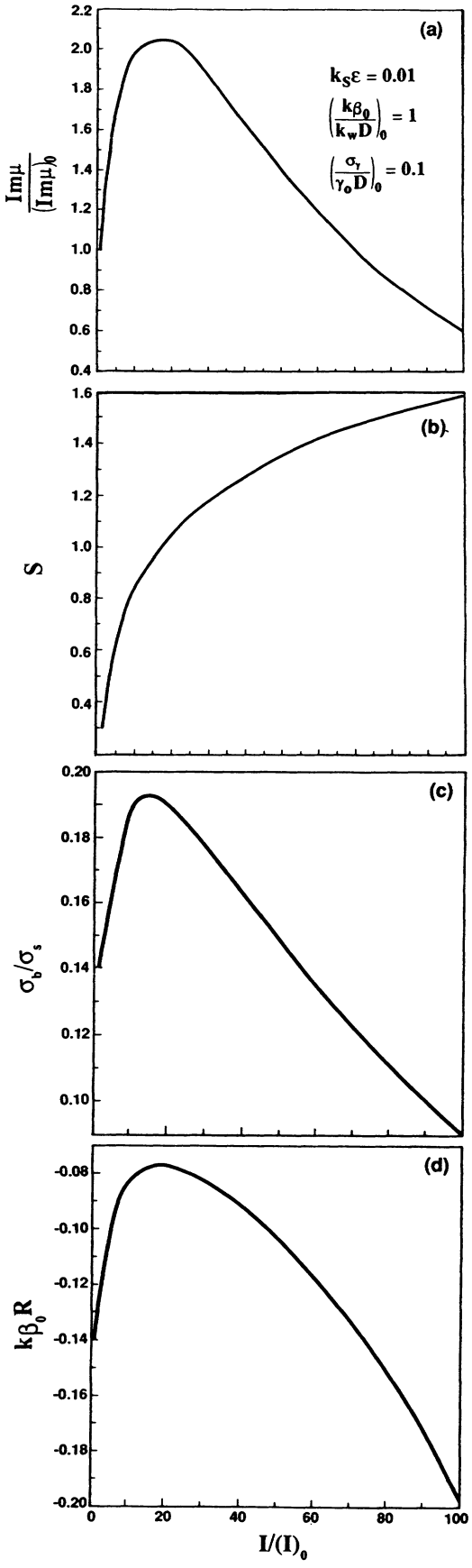

FIG. 1. Plot of (a) growth rate ratio $\mathrm{Im}\mu/(\mathrm{Im}\mu)_0$, (b) scaled thermal velocity S, (c) filling factor σ_b/σ_s, and (d) scaled radius of curvature $k_{\beta0}R$, vs current ratio $I/(I)_0$. In this case, scaled emittance $k_s\epsilon=0.01$. Prior to compression the electron beam is characterized by $(k_{\beta0}/k_w D)_0=1$, $(\sigma_\gamma/\gamma_0 D)_0=0.1$, and longitudinal compression leads to a monotonic transition to warm-beam interaction, as indicated by variation of S. Negative value of radius of curvature indicates diverging wave fronts along direction of propagation.

To see the effect of beam compression, Fig. 1(a) shows the ratio of the growth rate of the compressed beam to that of the uncompressed beam, $\mathrm{Im}\mu/(\mathrm{Im}\mu)_0$, as a function of the ratio of the current in the compressed beam to that in the uncompressed beam, $I/(I)_0$. Figure 1(a) shows that the maximum increase in the growth rate ratio is ≈ 2 and is obtained at $I/(I)_0 \approx 20$, beyond which $\mathrm{Im}\mu/(\mathrm{Im}\mu)_0$ declines due to kinetic effects. Insight into this behavior is provided in Fig. 1(b) which is a plot of S vs $I/(I)_0$. Observe that the maximum of $\mathrm{Im}\mu/(\mathrm{Im}\mu)_0$ occurs when $S \approx 1$. This corresponds to the spread in the axial velocity being comparable to the velocity difference between the beam and the ponderomotive wave. In other words, the ponderomotive wave is resonant with electrons in the bulk of the distribution. This is the warm-beam regime of interaction and a further increase in $I/(I)_0$ drives the interaction deeper into the kinetic regime, reducing $\mathrm{Im}\mu/(\mathrm{Im}\mu)_0$. It should be noted that for every current ratio the frequency is retuned by adjusting $1-\omega/ck_s$ in order to locate the *fastest* growing ponderomotive wave.

Figure 1(c) shows that the filling factor curve has a shape similar to the growth rate curve. The similarity is a consequence of operation in the gain-focusing regime. In particular, the higher the growth rate the smaller the radiation spot size σ_s, and hence the larger the filling factor. Figure 1(d) shows that the radius of curvature too has a dependence like that of the growth rate curve.

Another example of the effect of beam compression is shown in Figs. 2(a)–2(d). Figure 2(a) shows that the increase in the growth rate ratio is limited to ≤ 1.8, which is achieved at $I/(I)_0 \approx 10$. In Fig. 2(b) one observes an initial *drop* in the scaled thermal velocity, S, towards unity as the beam is compressed. This example may be understood by writing the S as

$$S = \frac{\{2(\sigma_\gamma/\gamma_0)^2 + [(k_{\beta 0}/k_w)k_s\epsilon]^2\}^{1/2}}{\eta}, \tag{5}$$

where $\eta \equiv -\mathrm{Re}\mu + (1-\omega/ck_s) - (k_{\beta 0}/k_w)k_s\epsilon$. Note that in the one-dimensional limit η is the cold-beam efficiency and scales as the cube root of the current [1]. The example in Fig. 2 displays the interplay between the various physical effects involved in the axial beam quality. A beam is said to be in the energy-spread- or in the emittance-dominated regime according to the relative magnitude of the terms in the numerator of Eq. (5). The example in Fig. 1 lies in the energy-spread-dominated regime. Figure 2, on the other hand, corresponds to the emittance-dominated regime where $S \approx (k_{\beta 0}/k_w)k_s\epsilon/\eta$.

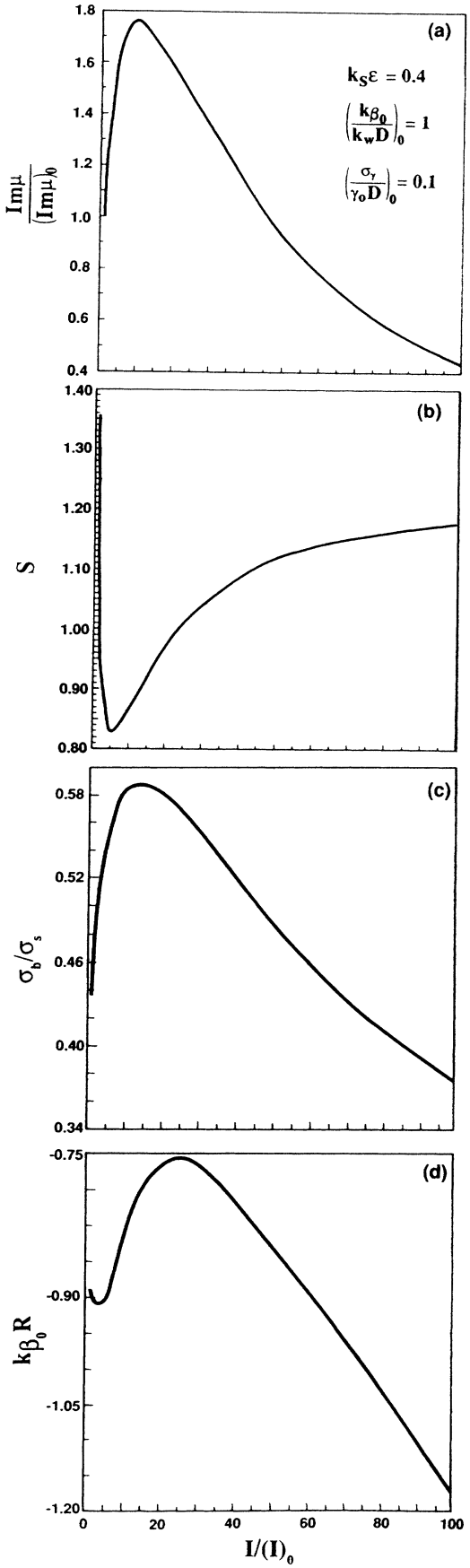

FIG. 2. Plot of (a) growth rate ratio $\mathrm{Im}\mu/(\mathrm{Im}\mu)_0$, (b) scaled thermal velocity S, (c) filling factor σ_b/σ_s, and (d) scaled radius of curvature $k_{\beta 0}R$ vs current ratio $I/(I)_0$. In this case, scaled emittance $k_s\epsilon = 0.4$. Prior to compression the electron beam is characterized by $(k_{\beta 0}/k_w D)_0 = 1$, $(\sigma_\gamma/\gamma_0 D)_0 = 0.1$, and longitudinal compression at first "improves" beam quality before leading to the warm-beam regime as indicated by variation of S. Variation of σ_b/σ_s and of $k_{\beta 0}R$ is indicative of the gain-focusing effect.

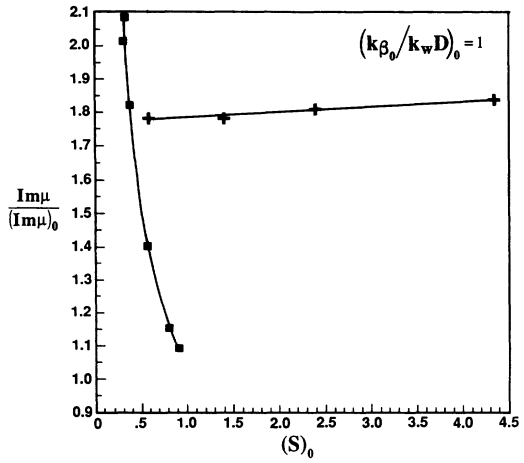

FIG. 3. Plot of growth rate ratio, $\mathrm{Im}\mu/(\mathrm{Im}\mu)_0$, versus scaled thermal velocity prior to compression, $(S)_0$, for $(k_{\beta 0}/k_w D)_0 = 1$. Energy-spread-dominated regime is indicated by solid squares and emittance-dominated regime is indicated by +'s.

The decrease in S is due to the effect of increased current on η, i.e., via the reactive part of the FEL interaction. An equivalent interpretation is to note that with increased current the *fastest* growing ponderomotive wave slows down and hence $\langle \beta_z - \beta_{ph} \rangle$ in the denominator of Eq. (1) increases. With the initial decline in S the interaction transitions towards the cold-beam regime and is therefore accompanied by the observed increase in $\mathrm{Im}\mu/(\mathrm{Im}\mu)_0$, even though initially the scaled thermal velocity exceeds unity. For sufficiently large compression ratios, however, $\sigma_\gamma/\gamma_0 D$ becomes the dominant term in the numerator of Eq. (5)—as was the case in Fig. 1—and S therefore increases with further compression, leading to the decline in $\mathrm{Im}\mu/(\mathrm{Im}\mu)_0$. Thus Fig. 2 illustrates an important point. That is, *FEL beam quality is governed not only by the emittance and energy spread on the beam but also by the current, through the reactive part of the interaction.* Figure 2(c) shows that the filling factor has a behavior similar to the growth rate curve. Figure 2(d) shows that the dependence of the radius of curvature on $I/(I)_0$ is similar to the growth rate curve although the peak is observed to occur at a larger compression ratio.

A number of examples of beam compression have been studied. Figure 3, where the peak growth rate ratio is plotted versus the scaled thermal velocity, summarizes the results. In the energy-spread-dominated regime, beam compression enhances the growth rate for $(S)_0 \leq 1$. Beyond $(S)_0 = 1$ compressing the beam causes a reduction in the growth rate rather than an increase. The situation is quite different in the emittance-dominated regime. In this regime there is always an increase in the growth rate ratio, independently of $(S)_0$. Figure 3 corresponds to the case where scaled wiggler amplitude, $(k_{\beta 0}/k_w D)_0$, is equal to unity. If the beam is sufficiently cold to begin with, the increase in the growth rate will be given by usual cold-beam scaling. The results of Fig. 3 apply when the cold-beam limit is not valid.

In summary, the effect of longitudinal beam compression on the spatial growth rate, scaled thermal velocity, filling factor, and radius of curvature of radiation wave fronts has been examined. We have found that (i) as the beam is longitudinally compressed to increase the current, the growth rate peaks and then drops off following transition into the warm-beam regime; (ii) the increase in growth rate depends on whether the beam is in the energy-spread- or the emittance-dominated regime; (iii) in the emittance-dominated regime compression always enhances the growth rate, the peak improvement in the growth rate being on the order of 2 for compression ratio in the range 10–20 in the examples here; and (iv) in the energy-spread-dominated regime beam compression enhances the growth rate provided the scaled thermal velocity is less than unity.

This work was supported by the Office of Naval Research.

*Permanent address: Icarus Research, 7113 Exfair Rd., Bethesda, MD 20814.

[1] C. W. Roberson and P. Sprangle, Phys. Fluids B **1**, 3 (1989).

[2] S. Takeda, K. Tsumori, S. Takamuku, T. Okada, K. Hayashi, and M. Kawanishi, Mem. Inst. Sci. Ind. Res., Osaka Univ. **43**, 27 (1986).

[3] B. E. Carlsten, D. W. Feldman, A. H. Lumpkin, J. E. Sollid, W. E. Stein, and R. W. Warren, Nucl. Instrum. Methods Phys. Res., Sect. A **272**, 247 (1988).

[4] W. E. Stein, W. J. D. Johnson, J. F. Power, and T. J. Russel, Nucl. Instrum. Methods Phys. Res., Sect. A **296**, 697 (1990).

[5] P. W. van Amersfoort *et al.*, Nucl. Instrum. Methods Phys. Res., Sect. A **304**, 163 (1991).

[6] P. Liger, G. A. Krafft, and D. Neuffer, Nucl. Instrum. Methods Phys. Res., Sect. A **318**, 290 (1992).

[7] C. Pellegrini *et al.*, Nucl. Instrum. Methods Phys. Res., Sect. A **331**, 223 (1993).

[8] C. W. Roberson, IEEE J. Quantum Electron. **21**, 860 (1985).

[9] B. Hafizi and C. W. Roberson, Phys. Rev. Lett. **68**, 3539 (1992).

[10] C. W. Roberson and B. Hafizi, Nucl. Instrum. Methods Phys. Res., Sect. A **331**, 365 (1993).